Aerofoil flow separation suppression using dimples

C. C. Beves
cbeves@hotmail.com
T. J. Barber and E. Leonardi
School of Mechanical and Manufacturing Engineering
University of New South Wales
Sydney, Australia

ABSTRACT

Flow separation is a source of aerodynamic inefficiency, by using vortex generators flow separation can be controlled. This is of particular benefit to flows around bodies which are susceptible to separated flows, such as bodies in ground effect. Previous studies on the ability of dimples to produce vortices for flow mixing concerned heat transfer applications. Experimental measurements using Laser Doppler Anemometry (LDA) were taken in the wake of the Tyrrell026 aerofoil ($Re_C = 0{\cdot}5 \times 10^5$) with a dimple array machined in the surface. Results for a dimple array of three rows placed forward of $x/c = 0{\cdot}23$ with $1{\cdot}5D$ dimple to dimple spacing, showed significant flow recovery in the wake. The velocity deficit of $u/U_{o,min} = -0{\cdot}1$ recovered to u/U_o,min = 0·3 with the dimple array and the size of the wake reduced by 50%; at $\alpha = 10^\circ$, $h/c = 0{\cdot}313$. The positive effect of the dimple array on the wing reduced as the wing was brought closer to the ground.

NOMENCLATURE

α	aerofoil angle of incidence
c	aerofoil chord
C_L	lift coefficient
C_D	drag coefficient
d_p	seeding particle diameter
D	dimple print diameter
δ	dimple depth
δ_{BL}	boundary-layer thickness
δ/D	dimple depth ratio
h	height from ground
h_{VG}	vortex generator height
h_{VG}/δ_{BL}	vortex generator height ratio
H	test section/channel height
h/c	ground clearance ratio
LDA	laser doppler anemometry
Re_C	wing chord Reynolds number
Re_D	dimple print Reynolds number
Re_H	test section/channel Reynolds number
Tu	turbulence intensity
u	streamwise 'x' velocity
u-RMS	streamwise 'x' RMS velocity
uu	turbulent normal stress
uu/U_o^2	normalised turbulent normal stress
uv	primary shear stress
uv/U_o^2	normalised primary shear stress
U_o	freestream velocity
Y_{norm}	distance normal to surface
y/c	vertical 'y' position from ground
$(y/c)^T$	$h/c = 0{\cdot}112$ translated to $h/c = 0{\cdot}313$
x/c	chordwise 'x' position along aerofoil

Paper No. 3624. Manuscript received 9 January 2010, revised version received 13 January 2011, accepted 1 February 2011.

https://doi.org/10.1017/S0001924000005856 Published online by Cambridge University Press

1.0 INTRODUCTION

The aerodynamics of bodies close to the ground have various real world engineering applications; aircraft in take-off, aircraft that operate at very low altitudes (Ekranoplan) and automotive aerodynamics. The ground proximity increases the demands on the design of a body due to the high velocity gradients and fluid shear stress between it and the ground. This causes increased sensitivity to flow separation even for a body with minimal lift capabilities or a wing with even a small angle of incidence, resulting in higher drag. Therefore being able to control the boundary layer with vortex generators in order to minimise the flow separation and drag is of interest, particularly as aerodynamic and fuel efficiency of vehicles increases in importance. The use of dimples as passive, sub-boundary-layer vortex generators has proven successful in improving heat exchanger design[1-5]. Applying this technique to a wing in ground effect may prove beneficial by increasing mixing very close to the surface.

Inverted wings in ground effect have the suction surface towards the ground, whereas a conventional lifting wing has the upper surface as the suction side. With the suction side towards the ground an aerofoil generates substantial negative lift (downforce) as well as an increase in drag. Data exist for inverted NACA aerofoil sections in ground effect[6,7,8] but the camber for these sections is usually lower than specially designed aerofoil sections for ground effect, such as the Tyrrell026 aerofoil. In recent years the Tyrrell026 profile has been studied and data for lift, drag and some limited information on the wake flow field is available[9,10,11]. For inverted aerofoils in ground effect, most generate higher downforce with reducing ground clearance 'h/c' until a point where the gain in downforce rapidly diminishes, known as the force reduction phenomenon. This height is dependent on how much lift force the aerofoil generates[8] and the higher the lift coefficient 'C_L' of the aerofoil the higher the ground clearance at which the force reduction occurs.

Results of the Tyrrell026 aerofoil across a broad range of angle of incidence 'α' (–3° to +15°) showed that the freestream aerofoil stalls very gradually[12], however, when brought to $h/c = 0{\cdot}313$ the aerofoil starts to stall abruptly and stall angle reduces as h/c is reduced. As the wing is brought closer to the ground, the accelerated flow causes increased peak suction and a higher pressure recovery demand[9]. At a critical ground clearance the pressure recovery is high and boundary-layer separation occurs near the trailing edge of the suction surface, even at $\alpha = 0°$. The migration of the separation point is highly dependent on reducing h/c[11]. Another important delineation being when there is no force reduction the aerofoil and ground boundary-layers do not merge[8].

Control of the boundary layer on the surface of the wing is possible by generating vortices either passively or actively. Numerous studies have investigated the benefits of passive vortex generation to improve the aerodynamic efficiency of aerofoils[13-22]. All of these studies confirm that boundary-layer protruding vortex generators provide near wall augmentations of shear stress and turbulence transport that are a result of vortex production. These vortices overcome the adverse pressure gradient on the surface such that the separation point will be delayed and the separation zone will be reduced[15,18]. The use of low profile vortex generators utilise the method of 'minimal near-wall protuberance' to produce vortices just strong enough to overcome baseline separation, although effective they are dependent on placement relative to the separation point[23].

Recent investigations into more efficient methods of passively generating vortices involve surface depressions using dimples[1,4,5,24-29]. The ability of the dimple to generate tornado-like vortices underneath the boundary layer poses significant advantages. Most studies consistently note the dimple draws in fluid from the side edges via a 'vacuum effect' which is entrained in the recirculation zone occupying the dimple and two lateral 'vortex cocoons' form from the dimple sides to the middle before periodically shedding vortices. The driving factors of the dimple to generate vortices are its depth to print diameter ratio 'δ/D' and the dimple based Reynolds number 'Re_D'[28,29]. As Re_D increases the flow inside the dimple becomes highly asymmetric, with one vortex dominating the other.

Experimental studies of dimple arrays focus on heat transfer applications[3,34,35]. Measurements of the friction factor of a smooth pipe with and without dimples indicated the friction factor increase was coupled to the dimple depth and spacing of the dimples to each other[3]. Upon analysing the effect of different cavity geometries in various channel configurations[30], it was shown that hemispherical dimples resulted in lower pressure drops compared to other types of cavities. This is due to the dimple vortex generation being organised rather than the more dissipative effect of shearing layers with boundary-layer protruding vortex generators[3]. The periodicity and organisation associated with the shedding of vortical fluid from individual dimples, is one of the primary features of dimpled surfaces[31].

There are other instances of utilising dimples in aerodynamic applications; golf balls[32,33] and dimpled tubine blades[34,35]. The results of the lift and drag of a spinning golf ball[32] indicated that dimpled balls showed a critical Reynolds number behaviour (the point of rapid C_D reduction) at lower Reynolds numbers than a smooth sphere. Both force measurements and hot-wire measurements inside golf ball dimples with no spin[33] showed that although the dimples were not deep enough to eject vortices, C_D still reduced by 50%. This was still possible as the dimples initiated instability along the separating shear layer, generating large turbulence intensity at the surface[33].

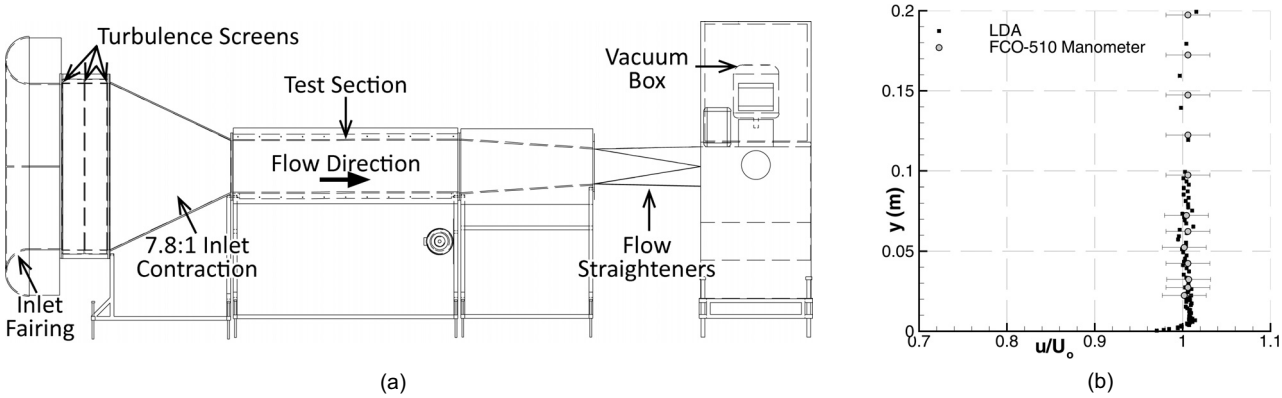


Figure. 1 (a) 235mm × 340mm UNSW wind-tunnel (b) Velocity profile in test section at x = 555mm.

https://doi.org/10.1017/S0001924000005856 Published online by Cambridge University Press

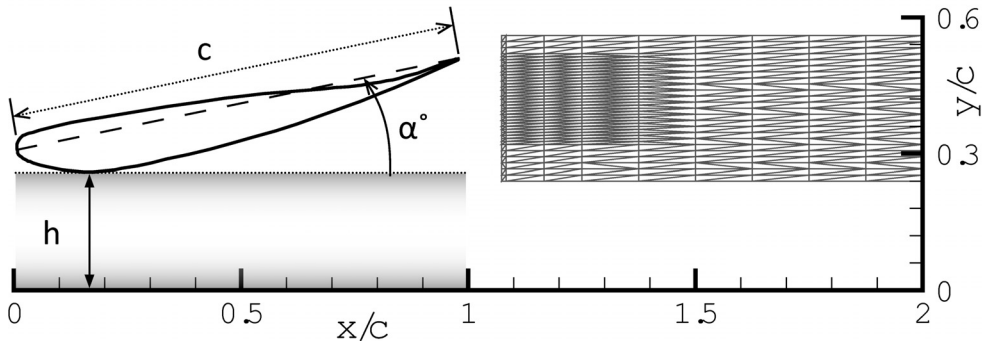


Figure 2. Experimental parameters and LDA grid in the tunnel centre plane.

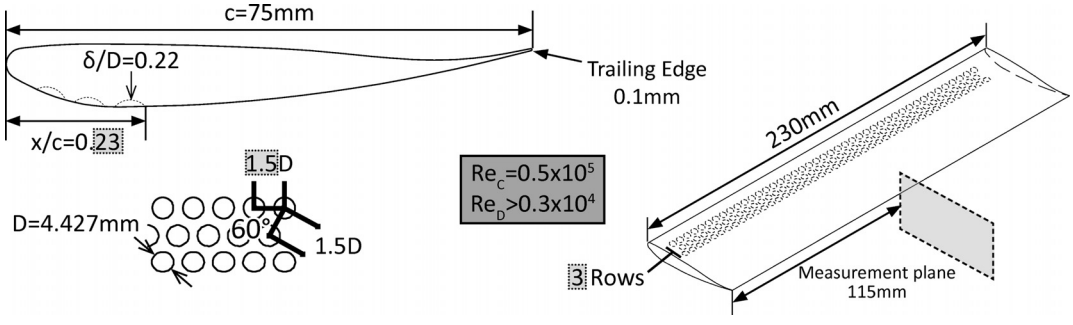


Figure 3. 1.5-3-23 Dimple array wing.

Work presented on the aerodynamic efficiency on a Pratt and Whitney PAK-B aerofoil section with one row of dimples showed that for all Reynolds numbers the presence of the dimples on the suction surface reduced separation losses[34]. Locating the dimples closest to the aerofoil separation point yielded the greatest reduction in the loss coefficient. The addition of a second row of dimples[35] increased turbulence intensity at the surface and moved blade separation further to the trailing edge, confirming that turbulent boundary-layers are able to follow surfaces better thus delaying separation[33,36].

The dimpled golf ball and turbine blade applications indicated a positive influence on drag, albeit it for low δ/D values which require more accurate placement relative to the boundary-layer separation point.

Results for small vortex generators of height 'h_{VG}' to boundary-layer thickness 'δ_{BL}' of $h_{VG}/\delta_{BL} < 0{\cdot}5$ indicated that stall angle can increase for slightly lower drag[23]. Thus increased aerodynamic efficiencies result by generating vortices with minimal boundary-layer protrusion, although placement is critical.

Previous studies show that dimple depth $\delta/D \approx 0{\cdot}2$ is a good compromise of efficient vortex production and low friction factor and pressure losses[3,37,38], thus $\delta/D = 0{\cdot}22$ will be used in this investigation. The placement of one row of dimples on the turbine blade[34] yielded lower pressure loss compared to standard vortex generators, thus more rows with a checkerboard pattern may yield further gains.

The underlying fluid mechanics of the wake are of interest here to prove the effectiveness of the dimple array. This preliminary performance study focuses on the direct influence the dimple array has on the wake of the Tyrrell026 aerofoil. As the ground clearance reduces, the influence the ground has on the fluid mechanics of the aerofoil increases. The size of the wake, its 'skew' towards the ground and the boundary-layer separation point are all entwined. Therefore influences of the surface modification due to the presence of the dimpled surface can be resolved in terms of flow structure differences by reductions in the wake size, velocity deficits, turbulence intensity and Reynolds stresses.

2.0 EXPERIMENTAL SETUP

The 235mm × 340mm UNSW open loop closed test section wind-tunnel used for the experimental measurements is shown in Fig. 1(a). The inlet has three turbulence damping screens positioned between the inlet fairing and the 7·8:1 contraction section. A 5Hp fan is used to draw the flow through the tunnel and flow straighteners are placed in the transition section into the vacuum box to counter the off axis orientation of the fan. The maximum test section speed is 10m^{-1}($\text{Re}_H = 3{\cdot}47 \times 10^5$, $\text{Re}_C = 0{\cdot}5 \times 10^5$). A KIMO TPL-3-100-T 3mm diameter integrated pitot tube and thermocouple is used to measure the differential pressure and temperature in the test section. It is connected to a Furness FCO510 Digital Micromanometer which is used to drive the vacuum box fan motor. The test section expansion ratio is such that boundary-layer growth does not impact on the freestream Reynolds number, pitot tube measurements indicate a 0·009% increase in freestream velocity over 600mm; test section flow angularity is less than 0·2°. Turbulence intensity in the test section inlet is 0·01% measured with the Laser Doppler Anemometry system.

The test section incorporates a raised moving ground that is powered by a 1·1kW motor, which is controlled by a Danfoss VLT6000 HVAC frequency converter. The angular velocity of the driving roller is measured using a US Digital 800·736.0194 encoder disc and a HEDS-9000 optical encoder. Belt tracking is a purely mechanical system and is calibrated to the desired speed. The velocity profile in the moving ground test section at the wing location (555mm from test section inlet) is shown in Fig. 1(b); δ_{BL} = 4·5mm.

Two wings were NC-machined from aluminium to the Tyrrell026 profile (75mm chord) which is a derivative of the LS(1)-0413 MOD profile[11]. The surface finish was left consistent to 800 grit sandpaper and not polished any further. Three rows of dimples were machined to $\delta/D = 0{\cdot}22$ with $D = 4{\cdot}427$mm and dimple centre to centre spacing

https://doi.org/10.1017/S0001924000005856 Published online by Cambridge University Press

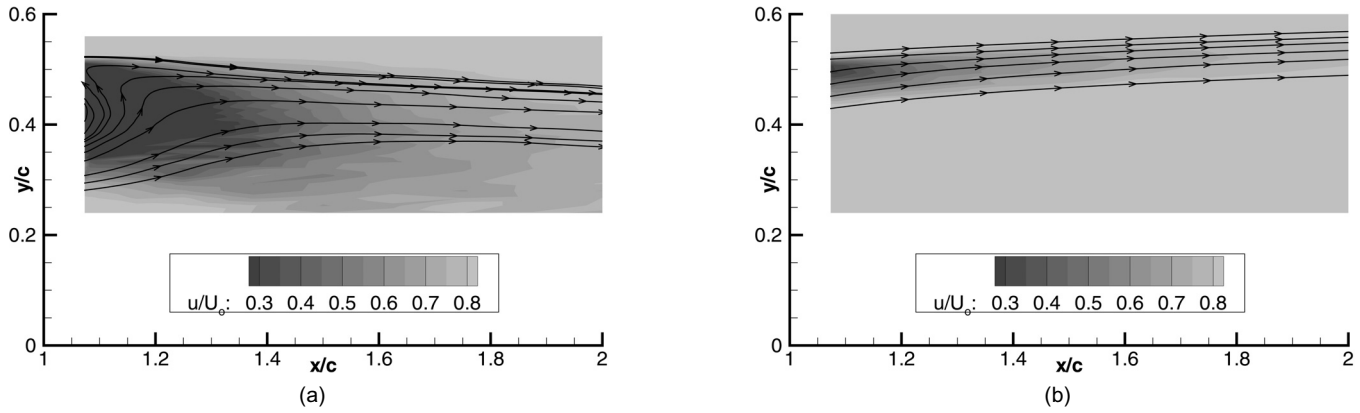


Figure 4. Streamlines and u/U_o contours for h/c = 0·313 (a) Clean wing (b) 1.5-3-23 Dimple array wing.

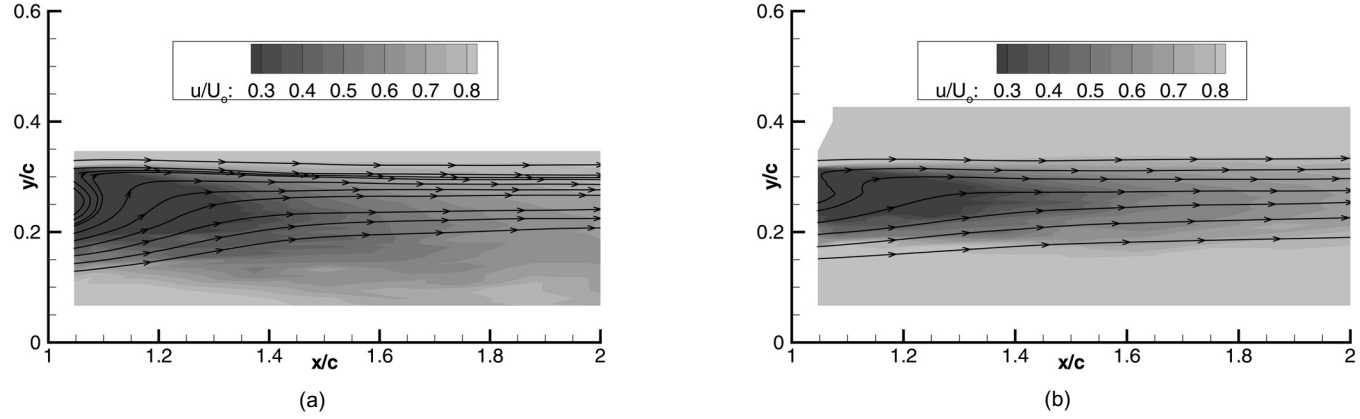


Figure 5. Streamlines and u/U_o contours for h/c = 0·112 (a) Clean wing (b) 1.5-3-23 dimple array wing.

Table 1
Experimental Error

Type	Source	Error
Spatial Error	Traverse	±0·01mm
	Wing Ground Clearance	±0·013%
	Wing Chord	±0·13%
	Dimple Diameter '*D*'	±0·25%
Velocity Measuement	Pitot tube	±1% for ±10°
	Hall Effect Sensor	±0·5%
	FCO-510 Manometer	±0·25%
LDA 95% confidence limit	u/U_o	±0·004
	uu/U^2_o	±0·0003
	uv/U^2_o	±0·0005

of 1·5*D* such that the dimples are equidistant in the array. The array is located forward of x/c = 0·23, forming the 1.5-3-23 dimple array wing modification shown in Fig. 3. Rather than make the whole lower surface dimpled the array was placed near the location of the peak suction to generate the most effective vortices in a targeted region so that the likely increase in skin friction is minimised. No fixed transition was used as it was deemed any potential flow augmentations of vorticity or turbulence as a result of the dimple array may be overwhelmed by producing more with a transition wire or strip. However, one set of measurements were conducted with a 0·15mm diameter trip wire at x/c = 0·23 the same location as the dimple placement. Two ground clearances of h/c = 0·313 and h/c = 0·112 were investigated and the angle of incidence 'α' was set at 10°, the LDA measurement plane in the wake is shown in Fig. 2, comprising a grid of approximately 350 points.

2.1 Measurement technique

Laser Doppler Anemometry (LDA) is a non-obtrusive measurement technique of flow velocities and turbulence statistics at a discrete point in a flow field that is seeded by particles. The LDA system used comprises a Coherent INNOVA 70C 5W Argon Ion laser supplying the primary beam to the DANTEC 60 × 41 transmitter box, which is an integrated colour separator and frequency shifter (Bragg Cell). This splits the primary beam into six separate beams into the DANTEC 60X24 fiber manipulators. The 85mm LDA probe heads emit six individual beams aligned using a CCD and operates in a three-dimensional, coincident, backscatter mode. The probe heads are mounted to a lightweight three axis traverse system controlled by an ISEL C142-4 Motor controller. Seeding is provided by a PivTec atomiser using vegetable oil with particle diameter '*dp*'=1μm, at 1bar gauge pressure, the particle slip velocity is less than 1% based on a previous analysis[42].

2.2 Uncertainty estimates

To ensure statistically independent, non-biased LDA velocity measurements, transit time weighting is applied which is consistently reliable for a range of data densities[39]. High data rates (> 1,500Hz 3D coincident) were achieved by a special technique of alignment using a CCD camera allowing beam alignment to a resolution approximately 50μm. The high level of LDA data rate, coupled with transit time weighted samples ensured that repeatability was consistent. Uncertainty values for turbulence measurements using LDA on a fluid flow with a normal distribution assumption using a 95% confidence level[40] are stated in Table 1 for the measurements taken. Measurement errors relating to the velocity readings and spatial errors with respect to NC-mill manufacturing

https://doi.org/10.1017/S0001924000005856 Published online by Cambridge University Press

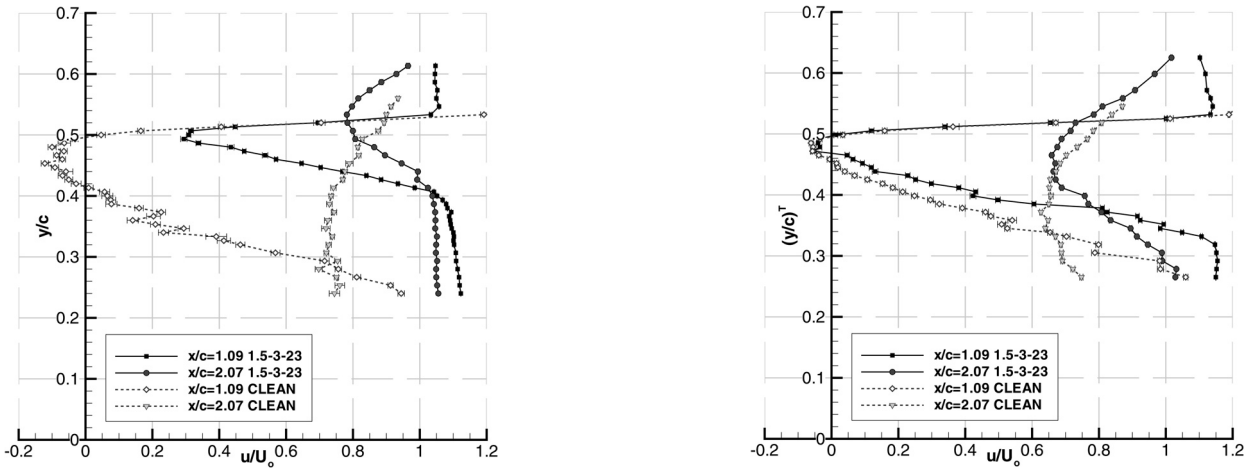


Figure 6. u/U_o velocity profile for clean wing and 1.5-3-23 Dimple array wing at (a) h/c = 0·313 and (b) h/c = 0·112.

tolerances of ±0·001mm and are outlined in Table 1. The error in using the Pitot tube and the Furness FCO-510 Digital Micromanometer to measure the aerofoil chord based Reynolds number 'Re_C' is 1·35%.

3.0 RESULTS AND DISCUSSION

Normalised streamwise velocity 'u/U_o' contours for the wing without dimples (clean) and with the 1·5-3-23 dimple array are shown in Figs 4 and 5 for h/c = 0·313 and h/c = 0·112 respectively. The wake reduction due to the dimple array is noticeable as the wake becomes thinner for both ground clearances of the wing. The greatest reduction in the size of the wake or its 'thickness' occurs for the 1·5-3-23 dimple array at h/c = 0·313 in Fig. 4(b). Pathlines released in the wake show the recirculation region immediately behind the aerofoil from $1 < x/c < 1{\cdot}2$ is minimised and for h/c = 0·313 in Fig. 4(b) there is no flow reversal. Additionally the vertical pathline deviation due to the upwash of the aerofoil is altered by the dimple array. For h/c = 0·313 the clean wing wake is still pulled down due to the ground influence in Fig. 4(a), yet for the dimple array there is noticeable upwash; Fig 4(b). The effect at h/c = 0·112 in Fig. 5(b) is less pronounced however the skew of the clean wing wake towards the ground is reduced, whereas with the dimple array there is a slight angle away from the ground. The aerofoil/ground boundary-layer interaction noted previously[8] appears to have been de-coupled due to the boundary-layer re-energising effect of the dimple array, which is greater at h/c = 0·313. It is still present at h/c = 0·112 in Fig. 5(b) with $u/U_o > 0{\cdot}85$ for $y/c < 0{\cdot}15$ and for the clean wing (in Fig. 5(a)) u/U_o is far less for $y/c < 0{\cdot}15$ over x/c = 1·03-2·07.

Figure 6 shows the direct comparison of velocity profiles in the wake at x/c = 1·09 and 2·07 for both the clean and dimple array wings. The velocity profiles at h/c = 0·112 are translated in the y direction so the trailing edge is equal to the h/c = 0·313 location '$(y/c)^T$', allowing a direct quantitative comparison. For h/c = 0·313 at x/c = 1·09 the minimum streamwise velocity '$u/U_{o,min}$' for the clean wing is –0·11, which increases to $u/U_{o,min}$ = 0·3 with the dimple array; at h/c = 0·112 there is minimal change from $u/U_{o,min}$ = –0·05. Accounting for the wake thickness as the change 'Δ' in (y/c) at u/U_o = 1 for the x/c = 1·09 velocity profile, in Fig. 6(a) for the clean wing $\Delta(y/c)$ = 0·3 and for the dimpled wing $\Delta(y/c)$ = 0·15, a 50% reduction. In Fig. 6(b) for the clean wing $\Delta(y/c)^T$ = 0·27 and for the dimpled wing $\Delta(y/c)^T$ = 0·23, a 15% reduction.

The changes of the wake velocity profile at x/c = 2·07 are less obvious for both ground clearances, yet velocity deficit recovers by $\Delta(u/U_{o,min})$ = 0·06 for h/c = 0·313 and $\Delta(u/U_{o,min})$ = 0·03 for h/c = 0·112. The upwash increase due to the dimple array results in the (y/c) location of $u/U_{o,min}$ increasing from (y/c) = 0·35 to (y/c) = 0·57 for h/c = 0·313 in Fig. 6(a) and from $(y/c)^T$ = 0·35 to $(y/c)^T$ = 0·48 for h/c = 0·112 in Fig. 6(b). Overall the increase of the velocity profile in the wake as a result of the dimple array is clear, there is substantial flow recovery at h/c = 0·313 and a marginal improvement in the wake between the ground and the aerofoil at h/c = 0·112, for $(y/c)^T < 0{\cdot}45$. The downstream improvement of the flow is such that the velocity profile is nearly uniform between the wake and the ground at α = 10° at both x/c positions for h/c = 0·313. There is less uniform flow between the wing and ground in Fig. 6(b) for h/c = 0·112, however it is evident the wake is no longer being pulled towards the ground and the flow beneath the wing at x/c = 1·09 is more consistent from $(y/c)^T < 0{\cdot}35$.

Given the changes to the wake structure in Figs 4 and 5 due to the dimpled aerofoil surface, a detailed measurement of the boundary layer on the suction side of the wing is useful to determine if the dimples are simply tripping the flow causing it to be attached to the surface longer. Figures 7 and 8 show the boundary-layer measurements of u/U_o and the fluctuating u-RMS velocity component read normal to the surface at two locations; x/c = 0·66 and x/c = 1. Three different wings were used, the clean wing with and without a fixed transition point (0·15mm tripwire at x/c = 0·23) and the 1·5-3-23 dimple array wing.

The differences in the velocity profiles are not substantial at h/c = 0·112, yet it is clear that the dimpled wing has the greater u/U_o profile to 4mm normal from the surface 'y_{norm}' in Fig. 7(a) and greater from 4mm away from the surface in Fig. 7(c). The fixed transition case lies somewhere in between the clean and the dimple wing at h/c = 0·112, yet the difference is greater at h/c = 0·313 in Figs 7(b) and 7(d). At h/c = 0·313 the flow separation is pronounced due to the negative streamwise flow close to the surface at x/c = 0·66 and x/c = 1, yet the dimple array noticeably increases to positive u/U_o through the measured y_{norm} range. It appears that the flow is quasi-stalled under the wing at h/c = 0·112, which does not change with the dimple array. At h/c = 0·313 the clean wing flow is separated and the addition of the dimples again recovers the flow underneath to a quasi-laminar-stalled flow regime.

Figure 8 shows more detail of the velocity fluctuation in the boundary layer. It is clear that with the dimple array the u-RMS velocity is more stable at a peak U-RMS value of 1·5-2·5m/sec and confined to 10mm from the surface. For the clean and transition cases there is a larger region of u-RMS > 4m/sec extending over 20mm normal to the surface. For the dimpled wing, u-RMS reduces to approximately 0 for y_{norm} > 15mm, which coincides with the increasingly uniform u/U_o profiles between the wing and ground in Fig. 7, indicating the dimples also improve the quality of the whole flow field between the wing and the ground, not just locally on the wing surface.

https://doi.org/10.1017/S0001924000005856 Published online by Cambridge University Press

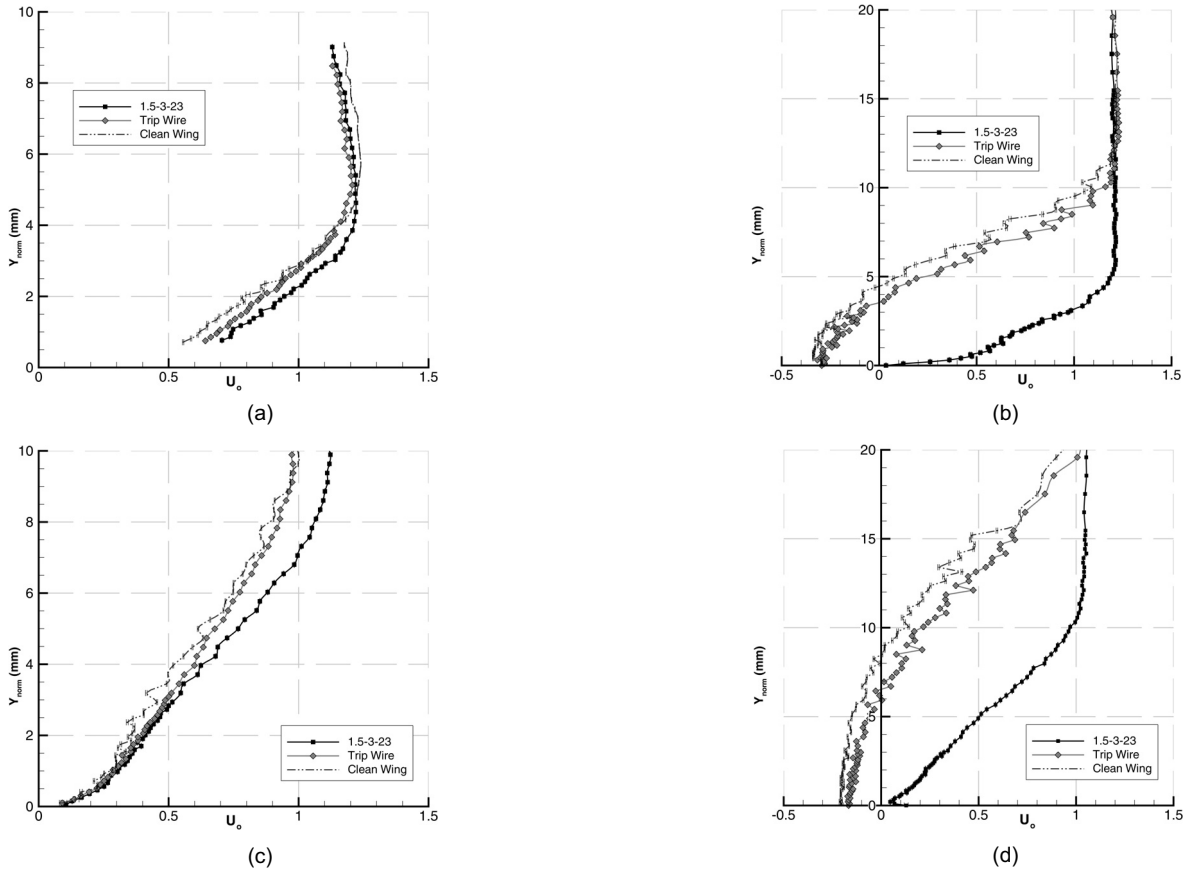


Figure 7. Boundary-layer u/U_o Velocity profile for; clean, tripwire and 1.5-3-23 Dimple array wing at:
(a) x/c = 0·66, h/c = 0·112 (b) x/c = 0·66, h/c = 0·313 (c) x/c = 1, h/c = 0·112 (d) x/c = 1, h/c = 0·313.

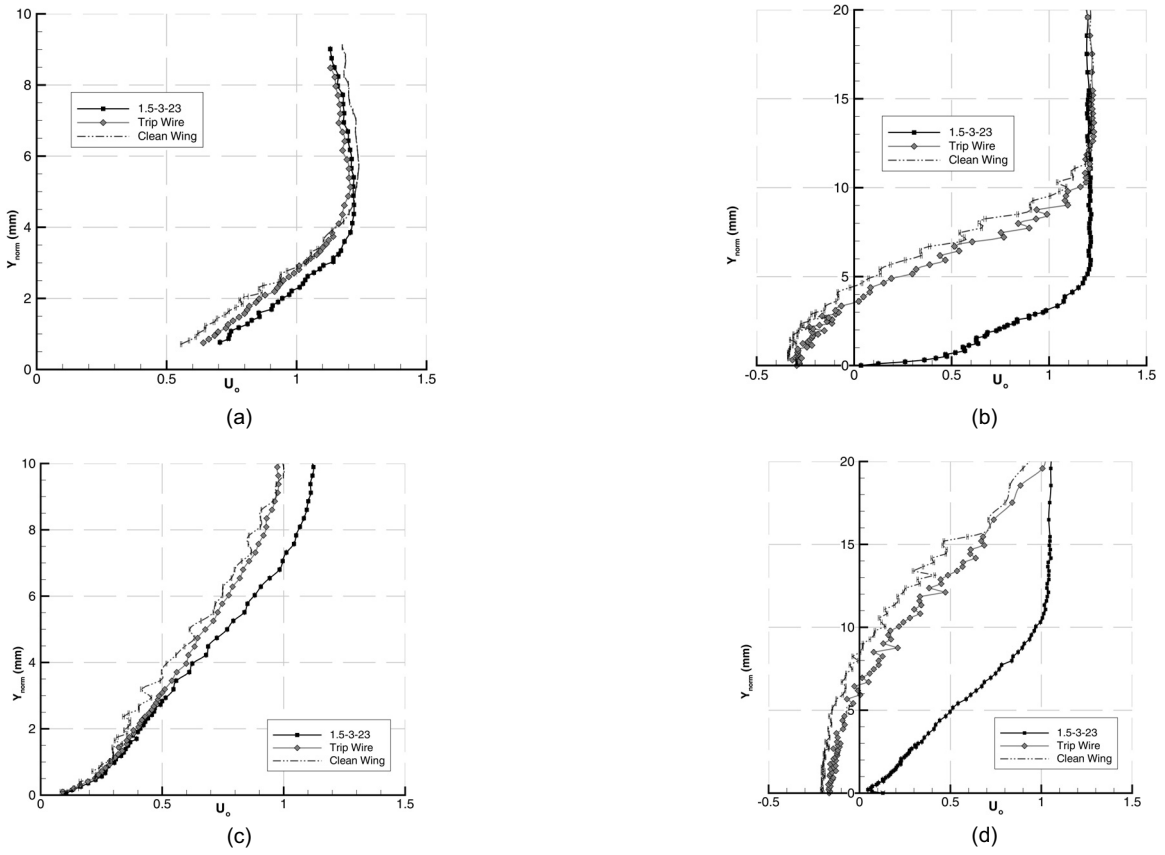


Figure 8. Boundary-layer u-RMS Profile for; Clean, Tripwire and 1.5-3-23 Dimple array wing at:
(a) x/c = 0·66, h/c = 0·112 (b) x/c = 0·66, h/c = 0·313 (c) x/c = 1, h/c = 0·112 (d) x/c = 1, h/c = 0·313.

https://doi.org/10.1017/S0001924000005856 Published online by Cambridge University Press

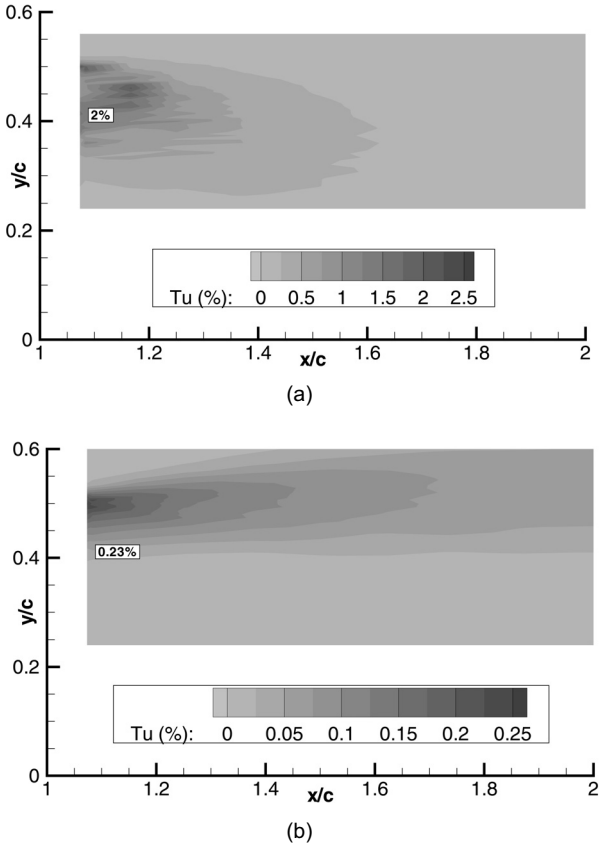


Figure 9. Turbulence Intensity contours at h/c = 0·313 for (a) Clean wing (b) 1.5-3-23 Dimple array wing.

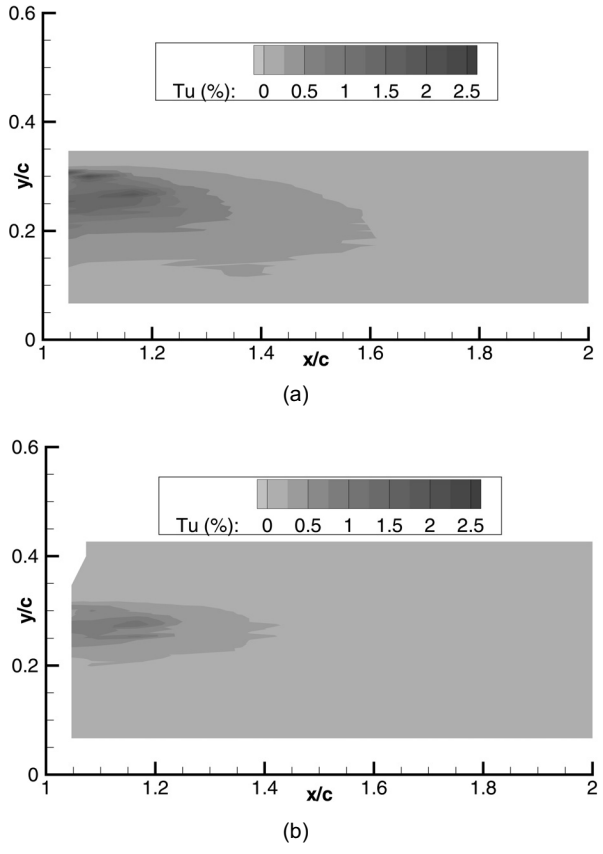


Figure 10. Turbulence Intensity contours at h/c = 0·112 for (a) Clean wing (b) 1.5-3-23 Dimple array wing.

The changes in the fluctuating streamwise velocity of Fig. 8 indicate that the higher order velocity measurements of turbulence intensity may also differ as a result of the dimple array. The turbulence intensity incorporating u' v' and w' is shown in the contour plots of Figs 9 and 10. At h/c = 0·313 in Fig. 9, the clean wing has a peak turbulence intenstity 'Tu' of 2%, which upon employing the dimpled surfacing reduces to 0·23%, and the trend of the large downward skewed wake becoming thinner with noticeable upwash follows on with the turbulence intensity contours. The region of higher turbulence intensity under the trailing edge of the wing at h/c = 0·112 decreases in size with the 1·5-3-23 dimple array wing in Fig. 10, yet the magnitude is roughly similar at $Tu \approx$ 1-1·5%. There are a few fluctuations of Tu > 2%, yet with the dimples ejecting vortices to suppress the flow separation the measurements indicate more stability of the wake turbulence and these peaks are not present.

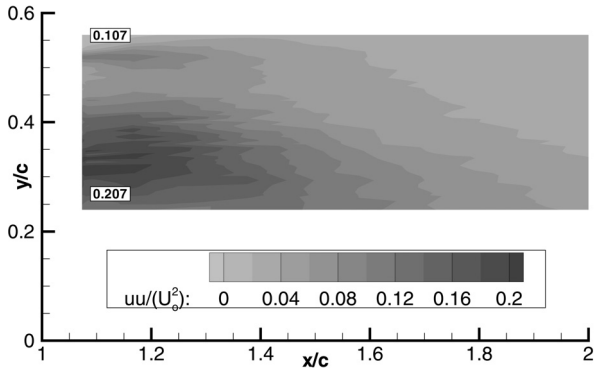
The in-plane Reynolds stresses are shown in Figs 11 to 14 for the normalised turbulent normal stress 'uu/U_o^2' and primary shear stress 'uv/U_o^2'. The turbulent normal stresses show two positive peaks, one thin region in the shear layer from the trailing edge of the aerofoil and another large, stronger region from the boundary-layer separation on the lower surface of the aerofoil. The primary shear stress has two concentrated areas with a negative and a positive value. The negative region is the stress placed on the fluid over the top of the aerofoil in the shear layer from the trailing edge as it is affected by the ground pulling the wake towards it. The large positive region is a direct effect of the upwash of the expanding region under the wing due to the camber of the aerofoil. The peak Reynolds Stress values are greater at h/c = 0·313 and dissipate quicker than h/c = 0·112. This is due to the moving ground being a barrier, confining the wake at low h/c to have less allowable downward vertical deviation or skew by the layer of fluid between the wing and round with increased velocity, limiting the wake to primarily dissipating longitudinally, stretching it out. It is likely the vortical shedding from the dimples is supressed by this faster fluid layer also, effectively squashing it back onto the wing surface and limiting its ability to generate vortices. Transient flow effects in the wake of a body in ground effect have previously been shown to reduce at low ground clearances[41]. The increased velocity under the wing compounds this further, the resultant being the ground providing an increased viscous damping effect on the wake.

Analysing the peak Reynolds stress values in the wake flow structure due to the boundary-layer separation on the aerofoil (the lower peak) in Figs 11 and 12, and not the structure due to the trailing edge shear layer indicates what effect the dimple array has on the flow beneath the aerofoil and the ground. Figures 11(b) and 12(b) indicate changes in the wake to reflect the thinner wake with noticeable upwash as seen in Fig. 4(b) and reductions of 86% for uu/U_o^2 and 76% for uv/U_o^2. At h/c = 0·112 in Figs 13 and 14, the peak Reynolds stress values reduce by 50% for both uu/U_o^2 and uv/U_o^2. It is interesting to note that although the Reynolds stress values are lower at lower h/c there is a limit to which the dimples can effectively act on reducing the stress in the wake and the boundary layer under the wing which is dependent on the ground proximity.

4.0 CONCLUSIONS

The Tyrrell026 aerofoil incorporating an array of three rows of dimples placed forward of x/c = 0·23 has proven to be effective in altering numerous aspects of the flow structure when placed in ground effect. Primarily the dimple array resulted in minimising the velocity deficit in the wake and reducing its size. The biggest improvement due to the dimple array occurred at h/c = 0·313, with the velocity deficit of $u/U_{o,min}$ = –0·11 increasing to $u/U_{o,min}$ = 0·3; the wake thickness also reduced 50%. At h/c = 0·112 there is minimal change from the velocity deficit of $u/U_{o,min}$ = –0·05, however the

https://doi.org/10.1017/S0001924000005856 Published online by Cambridge University Press



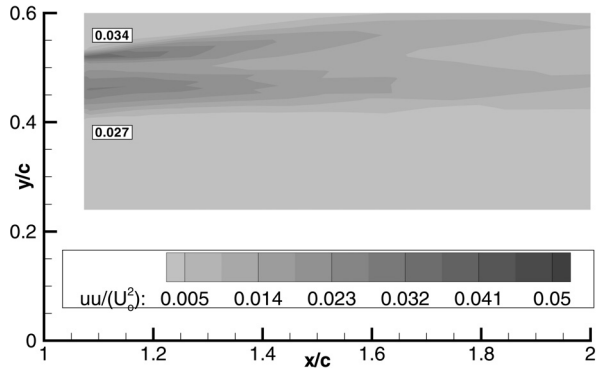
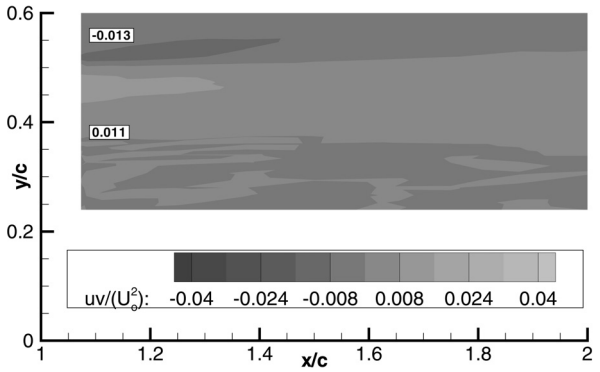


Figure 11. Turbulent normal stress contours at h/c = 0·313 for (a) Clean wing (b) 1.5-3-23 Dimple array wing.



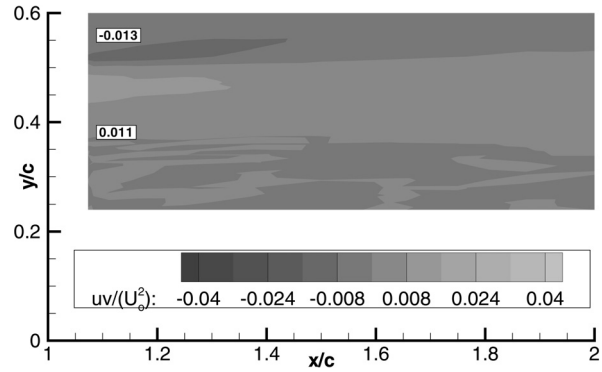
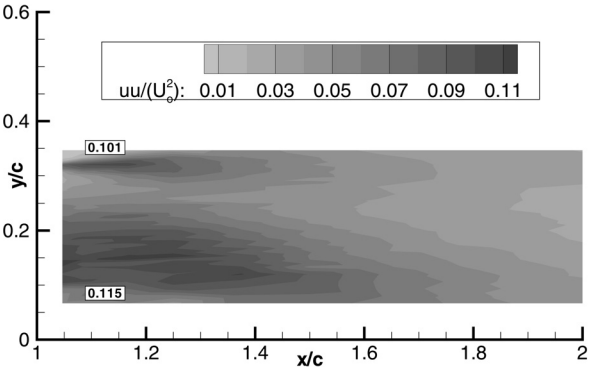


Figure 12. Primary shear stress contours at h/c = 0·313 for (a) Clean wing (b) 1.5-3-23 Dimple array wing.



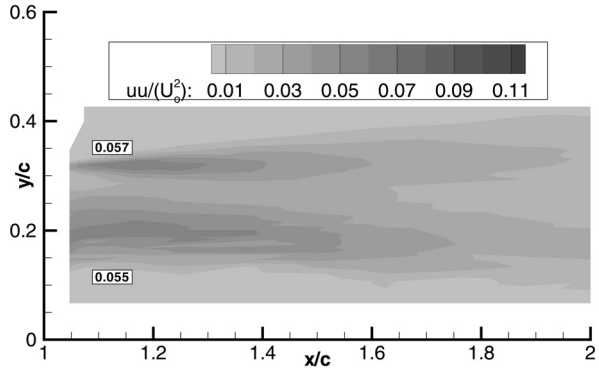
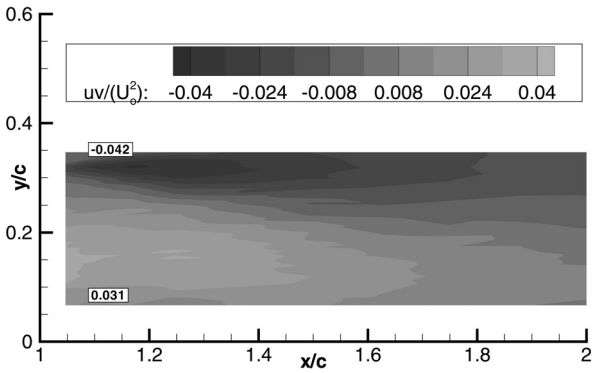


Figure 13. Turbulent normal stress contours at h/c = 0·112 for (a) Clean wing (b) 1.5-3-23 Dimple array wing.



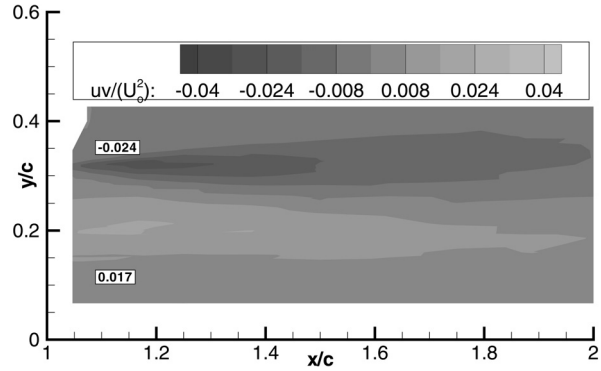


Figure 14. Primary shear stress contours at h/c = 0·112 for (a) Clean wing (b) 1.5-3-23 Dimple array wing.

https://doi.org/10.1017/S0001924000005856 Published online by Cambridge University Press

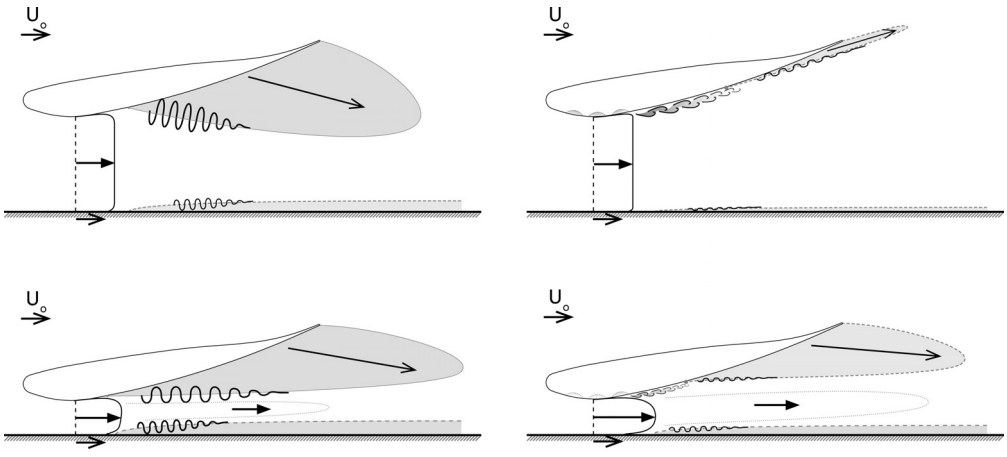


Figure 15. Effect of dimple array with reducing *h/c* on Tyrrell026 Aerofoil a) Clean and b) 1.5-3-23 dimple array.

wake thickness still reduced by 15%. The dimpled aerofoil at higher ground clearance no longer showed the downward skew of the wake as a result of the ground, the dimples effectively energising the aerofoil boundary-layer to an extent as to de-couple it from the ground effect and produce upwash. The downstream improvement of the flow is such that the velocity profile is nearly uniform between the wake and the ground at $h/c = 0{\cdot}313$.

Measurements of the boundary layer on the dimpled wing and on the clean wing with and without a transition wire indicated that the dimples are not simply tripping the boundary layer to turbulent and keeping it attached longer, they are actually generating strong enough vortices to reattach the flow for the majority of the lower wing surface. The added secondary benefits of this are the lower wake turbulence intensities and turbulent normal stress and primary shear stress Reynolds stress components, yielding improved flow in the immediate location surrounding and beneath the wing and also downstream.

The generation of organised vortices from the dimple array is clearly demonstrated at $h/c = 0{\cdot}313$ by the flow separation suppression in the wake. However all of the reductions in wake size, velocity deficit, skew, turbulence and Reynolds stress components due to the presence of the dimple array decreased in effectiveness as the ground clearance reduced. At the higher ground clearance the boundary layer of the clean wing has a higher velocity fluctuation (see Fig. 8), and in turn higher shedding frequency. This reduces for lower ground clearance as the ground proximity (and the layer of higher velocity fluid between the wing and ground) constrains the suction surface boundary-layer and wake to a greater degree and limits these fluctuations from the interference with the ground; effectively dampening them. With the addition of the dimples and the ability they have to shed organised vortical structures the vortices generated at the lower ground clearance are overwhelmed by the higher speed flow between the wing and the ground, limiting their effectiveness even through Re_D has increased; Fig. 15.

The investigation into utilising dimples to supress flow separation has indicated substantially improved flow both in the wake and beneath the wing and the ground. With such significant flow structure changes it is likely that the resultant lift and drag forces will also be altered. The improved flow conditions between the wing and the ground are likely to result in higher downforce generation of the dimpled wing due to the higher speed flow and resultant lower pressure. The expected increase in skin friction of the dimpled aerofoil would be offset by the large reductions in pressure drag, particularly as at $h/c = 0{\cdot}313$ the wake is no longer separated. Therefore given the substantial improvements to the flow both behind and beneath the aerofoil it is likely the dimpled aerofoil has increased aerodynamic efficiency. Full scale testing focussing on aerodynamic force measurement is essential to determine the suitability of the dimple array to act as highly efficient vortex generators. The low Reynolds number used in this study may render the exact geometry ineffective at a higher Reynolds number; however the concept of specifically targeting a few rows of dimples (with $\delta/D = 0{\cdot}22$) that are large enough to eject strong vortices has been shown to minimise flow separation and improve the flow under the wing when placed in an optimal position relative to the flow separation point.

REFERENCES

1. LIGRANI, P.M. Flow visualization and flow tracking as applied to turbine components in gas turbine engines, *Meas Sci Tech*, 2000, **11**, pp 992-1006.
2. ISAEV, S.A. and LEONT'EV, A.I. Analysis of the effect of viscosity on the vortex dynamics at laminar separated flow past a dimple on a plane with allowance for its asymmetry, *J Engineering Physics and Thermophysics*, 2001, **74**, (2), pp 339-346.
3. BUNKER, R.S. and DONNELLAN, K.F. Heat transfer and friction factors for flows inside circular tubes with concavity surfaces, Proc. ASME Turbo Expo, 16-19 June 2003, Atlanta, Georgia, US.
4. KHALATOV, A.A. and BYERLEY, A. Flow characteristics within and downstream of spherical and cylindrical dimple configurations on a flat plate under laminar flow conditions, Proc. of the ASME Turbo Expo, Vienna, Austria, 14-17 June 2004, ASME Paper No. GT2004-53656.
5. LIGRANI, P.M. and PARK. J. Numerical predictions of heat transfer and fluid flow characteristics for seven different dimpled surfaces in a channel, *Num Heat Transfer (Part A)*, 2005, **47**, pp 209-232.
6. RAZENBACH, R. and BARLOW, J.B. Two-dimensional aerofoil in ground effect, an experimental and computational study, SAE, 1994, SAE 942509.
7. RAZENBACH, R. and BARLOW, J.B. Cambered aerofoil in ground effect, an experimental and computational study, SAE, 1996, 960909.
8. RAZENBACH, R. and BARLOW, J.B. Multi-element aerofoil in ground effect- an experimental and computational study, AIAA, 1997, AIAA-97-2238.
9. ZHANG, X. and ZERIHAN, J. Off-surface aerodynamics measurements of a wing in ground effect, *J Aircr*, 2003, **40**, (4), pp 716-725.
10. MORYOSSEF, Y. and LEVY, Y. Effect of oscillations on aerofoils in close proximity to the ground, *AIAA J*, 2004, **42**, (9), pp 1755-1764.
11. MAHON, S. and ZHANG, X. Computational analysis of pressure and wake characteristics on an aerofoil in ground effect, ASME, 2005, **127**, pp 290-298.
12. ZERIHAN, J. An Investigation into the Aerodynamics of Wings in Ground Effect, PhD Thesis, University of Southampton, School of Engineering, 2001.

https://doi.org/10.1017/S0001924000005856 Published online by Cambridge University Press

13. NICKERSON, J.D. A study of vortex generators at low Reynolds numbers, AIAA, 1986, AIAA-86-0155.
14. LIN, J.C. and HOWARD, F.G. Investigation of several passive and active methods for turbulent flow separation control, 21st AIAA Fluid Dynamics, Plasma Dynamics and Lasers Conference, 1990, p 21.
15. LIN, J.C. and ROBINSON, S.K. Separation control on high Reynolds number multi-element aerofoils, 10th Applied Aerodynamics conference, 1992, AIAA-1992-2636.
16. STORMS, B.L. Lift enhancement of an aerofoil using a gurney flap and vortex generators, *J Aircr*, 1994, **31**, (3), pp 542-547.
17. STORMS, B.L. and ROSS, J.C. Experimental study of lift enhancing tabs on a two-element aerofoil, *J Aircr*, 1995, **32**, (5), pp 1072-1078.
18. KLAUSMEYER, S.M. A flow physics study of vortex generators on a multi-element aerofoil, 34th aerospace sciences meeting and exhibit, 1996, AIAA-1996-548.
19. ISAEV, S.A. and SUDAKOV, A.G. Effect of supercirculation in a flow around a thick aerofoil with vortex cells, *Doklady Physics*, 2001, **46**, (3), pp 199-201.
20. RAE, A.J., GALPIN, S.A. and FULKER, J. Investigation into the scale effect on the performance of sub boundary-layer on civil aircraft high-lift devices, 2nd Flow Control Conference, AIAA, 2002, AIAA-2002-3274.
21. LEE, H-T. and KROO, I.M. Computational Investigation of wings with miniature trailing edge control surfaces, 2nd AIAA Flow Control Conference, AIAA, 2004, AIAA-2004-2693.
22. VAN DER BERG, J.W., MASELAND, J.E.J. and BRANDSMA, F.J. Low speed maximum lift and flow control, *Aerospace Science and Technology*, 2004, **8**, pp 389-400.
23. LIN, J.C. Review of research on low profile vortex generators to control boundary-layer separation, *Progress in Aerospace Sciences*, 2002, **38**, pp 389-420.
24. MAHMOOD, G.I. and LIGRANI, P.M. Heat transfer in a dimpled channel: combined influences of aspect ratio, Reynolds number and flow structure, *Int J of Heat and Mass Transfer*, 2002, **45**, pp 2011-2020.
25. CHEW, Y.T. and KHOO, B.C. Flow visualization studies on flow structures within spherical dimples of different depths with/without round edges, Proceeding of 5th PSFVIP, 2005, PSFVIP-5-280.
26. ISAEV, S.A. and LEONT'EV, A.I. Numerical study of the eddy mechanism of enhancement of heat and mass transfer near a surface with a cavity, *J Engineering Physics and Thermophysics*, 1998, **71**, (3), pp 481-487.
27. ISAEV, S.A. and LEONT'EV, A.I. Identification of self-organized vortex like structures in numerically simulated turbulent flow of a viscous incompressible liquid streaming around a well on a plane, *Technical Physics Letters*, 2000, **26**, (1), pp 15-18.
28. ISAEV, S.A. and LEONT'EV, A.I. Modelling of the influence of viscosity on the tornado heat exchange in turbulent flow around a small hole on the plane, *J Engineering Physics and Thermophysics*, 2002, **75**, (4), pp 890-898.
29. ISAEV, S.A. and LEONT'EV, A.I. Numerical analysis of the influence of the depth of a spherical hole on a plane wall on turbulent heat exchange, *J Engineering Physics and Thermophysics*, 2003, **76**, (1), pp 61-69.
30. BUNKER, R.S. and M. GOTOVSKII, M. Heat transfer and pressure loss for flows inside converging channels with surface concavity effects, Proc of 4th Int Conf Compact Heat Exchangers and Enhancement Tech, Begell House, New York, US, 2003.
31. LIGRANI, P.M. and HARRISON, J.L. Flow structure due to dimple depressions on a channel surface, *Physics of Fluids*, 2001, **13**, (11), pp 3442-3451.
32. BEARMAN, P.W. and HARVEY, J.K. Golf ball aerodynamics, *Aeronaut Q*, 1976, **27**, (2), pp 112-122.
33. CHOI, J., JEON, W-P. and CHOI, H. Mechanism of drag reduction by dimples on a sphere, *Physics of Fluids*, 2006, **18**, 041702, pp 1-4.
34. LAKE, J.P. and KING, P.I. Low Reynolds number loss reduction on turbine blades with dimples and V-Grooves, AIAA, 2000, AIAA-00-0738.
35. RIVIR, R.B. and SONDERGAARD, R. Control of separation in turbine boundary-layers, 2nd AIAA Flow Control Conference, 2004, AIAA 2004-2201.
36. DAVIES, J.M. The aerodynamics of golf balls, *J of Applied Physics*, 1949, **20**, (9), pp 821-828.
37. LIGRANI, P.M., WON, S.Y. and ZHANG, Q. Comparisons of flow structure above dimpled surface with different dimple depths in a channel, *Phys of Fluids*, 2005, **17**, pp 3442-3452.
38. WON, S.Y. and LIGRANI, P.M. Numerical predictions of flow structure and local Nusselt number ratios along and above dimpled surfaces with different dimple depths in a channel, Num. *Heat Transfer (Part A)*, 2004, **46**, pp 549-570
39. ALBRECHT, H.E., BORYS, M., DAMANSHKE, N. and TROPEA, C. *Laser Doppler and Phase Doppler Measurement Techniques*, Springer, New York, US, 2003.
40. BENEDICT, L.H. and GOULD, R.D. Towards better uncertainty estimates for turbulence statistics, *Exp in Fluids*, 1996, **22**, pp 129-136.
41. KIM, M.S. and GEROPP, D. Experimental investigation of the ground effect on the flow around some two dimensional bluff bodies with ground effect, *J Wind Engineering and Industrial Aerodynamics*, 1998, **74-76**, pp 511-519.
42. RAFFEL, M., WILLERT, C. and KOMPENHAUS, *J. Particle Image Velocimetry: A Practicle Guide*, Springer, New York, US, 1998.

https://doi.org/10.1017/S0001924000005856 Published online by Cambridge University Press